Indonesian Physical Review
Volume 09 Issue 03, September 2026
P-ISSN: 2615-1278, E-ISSN: 2614-7904

Optical, Corrosion, and Electrochemical Analysis of Graphite–Turmeric Extract Formulations for Zinc in 3.5 wt.% NaCl Solution

Romi Fadli Syahputra[1*], Neneng Fitrya[1], Delovita Ginting[1], Fauzan Fahturrahman[1], Salsabila Marcela[1], Aas Wiranda[1], Salsabillah Ratih Putri[1], Putri Fitri Handayani[1], Bunga Meyzia[2], Zulkarnain Zulkarnain[3]

[1] *Department of Physics, Faculty of Mathematics, Natural Science, and Health, Universitas Muhammadiyah Riau, Indonesia*
[2] *MJIIT, Universiti Technologi Malaysia, Malaysia*
[3] *Department of Physics, Faculty of Mathematics and Natural Science, Universitas Riau, Indonesia*

Corresponding Author's E-mail: romifadli@umri.ac.id

Article Info

Article info:
Received: 19-01-2026
Revised: 12-07-2026
Accepted: 15-07-2026

Keywords:
Corrosion rate; Inhibitor corrosion; Graphite; Curcuminoids

How To Cite:
R. F. Syahputra, N. Fitrya, D. Ginting, F. Fathurrahman, S. Marcela, A. Wiranda. S. R. Putri. P. F. Handayani, B. Meyzia, Zulkarnain, "Optical, Corrosion, and Electrochemical Analysis of Graphite–Turmeric Extract Formulations for Zinc in 3.5 wt.% NaCl Solution", Indonesian Physical Review, vol. 9, no. 3, p 503-517, 2026.

DOI:
https://doi.org/10.29303/ipr.v9i3.649.

Abstract

The development of environmentally friendly corrosion protection materials is important for protecting metallic components exposed to saline environments. In this work, graphite–curcuminoids hybrid formulations based on curcuminoids extracted from Curcuma longa *and graphite (IGC) were evaluated for corrosion protection of zinc in 3.5 wt.% NaCl solution. Optical properties were characterized by UV–Vis spectroscopy, while corrosion behavior was assessed using linear sweep voltammetry and Tafel polarization analysis. The incorporation of graphite modified the absorption characteristics of curcuminoids and slightly reduced the optical band gap from 2.65 eV (curcuminoids) and 2.85 eV (graphite) to 2.59–2.62 eV for the hybrid formulations. Among the investigated compositions, IGC1 exhibited the best performance, reducing the corrosion rate from 0.1175 to 0.0408 mm/y and achieving an inhibition efficiency of 65.3%. In contrast, IGC2 showed a higher corrosion rate of 0.1863 mm/y, indicating that excessive graphite loading adversely affected the protective performance. The results indicate that the corrosion behavior of graphite–curcuminoids hybrid formulations is highly dependent on composition. These findings demonstrate the potential of graphite–curcuminoids hybrids as environmentally friendly corrosion inhibitors for zinc in saline water media.*

Copyright (c) 2026 by Author(s). This work is licensed under a Creative Commons Attribution-ShareAlike 4.0 International License.

Introduction

The increasing demand for durable and environmentally friendly metallic systems in electrochemical and industrial environments has intensified research into efficient corrosion protection strategies. Corrosion not only degrades metallic components but also significantly reduces the performance, efficiency, and service life of electrochemical devices and structural materials [1]. Among various protection methods, the use of organic corrosion inhibitors has attracted considerable attention due to their cost-effectiveness, ease of application, and minimal environmental impact [2], [3].

Natural organic compounds derived from plant extracts have emerged as promising green corrosion inhibitors. Curcuminoids, the main bioactive compound in turmeric (*Curcuma longa*), have been widely reported as an effective corrosion inhibitor owing to their rich π-electron system and functional groups such as hydroxyl and carbonyl moieties [4], [5]. These functional groups facilitate strong adsorption on metal surfaces through both physical and chemical interactions [6]. While curcumin is known as an effective organic corrosion inhibitor, its relatively poor film robustness and limited interfacial stability in chloride media may reduce long-term protection performance [7].

Carbon-based materials such as graphite have been extensively studied for corrosion protection due to their high electrical conductivity, chemical stability, and ability to participate in π–π interactions [8]–[11]. Graphite and graphene derivatives have demonstrated good corrosion inhibition performance by forming protective layers on metallic substrates [9], [12], [13]. Nevertheless, their relatively weak adhesion and poor dispersion in aqueous environments often limit their long-term effectiveness.

To address these limitations, a hybrid graphite–curcuminoids system is proposed as a potential corrosion protection strategy. The synergistic interaction between organic molecules and conductive carbon materials is expected to enhance adsorption strength, improve electronic interactions, and stabilize the protective film formed on the metal surface [9]. In addition, understanding the optical and electronic properties of such hybrid systems is essential, as these properties are closely related to charge transfer behavior and adsorption mechanisms [14].

In this study, we investigate the optical properties of graphite–curcuminoid inhibitor (IGC) systems using UV–Vis spectroscopy, including band-gap estimation and spectral deconvolution. Potentiodynamic polarization measurements evaluated the corrosion inhibition performance of different formulations in a 3.5 wt% NaCl solution. A qualitative comparison of the optical and electrochemical results was conducted to examine possible relationships between the optical characteristics of the hybrid systems and their corrosion behavior. As an initial investigation, this work aims to provide a rapid assessment of the potential of graphite–curcuminoids dual inhibitors for mitigating corrosion of zinc electrodes, which are considered promising anode materials for sodium-ion batteries [1], [3].

Experimental Method

Materials and reagents

Curcuminoids were extracted from fresh turmeric rhizomes, while commercial graphite powder was used as the conductive component. Sodium chloride (NaCl) (Merck), ethanol, and

deionized (DI) water were used as received. Metallic substrates, including zinc (Zn) (from the marketplace), are employed as working electrodes. Epoxy resin was used to isolate non-exposed electrode surfaces during electrochemical measurements.

Extraction of curcuminoids

Fresh turmeric rhizomes (200 g) were thoroughly cleaned, crushed, and subjected to maceration using ethanol as the solvent for 72 h at room temperature [4]. The mixture was then filtered to remove solid residues, and the resulting curcuminoids-rich extract was stored in a sealed container for further use. This extraction method is known to preserve the molecular structure and optical activity of curcuminoids.

Preparation of inhibitor solutions

The inhibitor solutions were prepared by mixing curcuminoid extract with graphite powder in ethanol. 5 ml of curcuminoid extract was dissolved in 20 ml of ethanol, and 5 ml of this solution was applied (labeled as CUR solution). For making a graphite solution, 1 g of graphite is dispersed in 10 mL of ethanol. Then about 0.1 ml of this solution is diluted in 70 ml of ethanol for the application, denoted as GR suspension. The visual appearance of the prepared inhibitor formulations is displayed in Figure 1, corresponding to the compositions detailed in Table 1. The CUR sample has a yellowish color, typical for curcuminoid extract, while the graphite solution has a grayish color. For the composite formulations (IGC1, IGC2, and IGC3), the physical blending of the yellow organic extract with the dark graphite dispersion yields a characteristic soft greenish-gray color, visually confirming the physical incorporation of the graphite particles into the organic matrix.

Table 1. The inhibitor composition for the application

Sample	CUR (ml)	GR (ml)	Ethanol (ml)	Total volume (ml)
CUR	10	-	-	10
GR	-	10	-	10
IGC1	5	1	5	11
IGC2	5	2	5	12
IGC3	5	3	5	13

Figure 1. The visual of graphite, curcuminoids, and graphite–curcuminoids inhibitor solutions.

Application of an inhibitor to the electrode

Prior to inhibitor application, metal electrodes were mechanically polished using 1000-grit sandpaper, rinsed with DI water, and dried. The non-exposed surfaces were coated with epoxy

resin, leaving an exposed area of approximately 1 cm². The electrodes were immersed in the IGC solution for 10 minutes at room temperature to allow adsorption of inhibitor molecules onto the metal surface [15].

Microwave-assisted surface activation

After immersion, the coated electrodes were irradiated with microwave energy for 1 min using a commercial microwave oven (Sharp R-728). The device operates at 2.45 GHz with a maximum output power of 900 W (220 V, 50 Hz). Microwave treatment was employed to enhance surface activation, improve inhibitor adhesion, and promote stronger interfacial interactions between the inhibitor and the metal surface [16]–[18]. Upon the completion of the short exposure cycle, empirical inspection confirmed that the sample surfaces were thoroughly dry and solidified. Due to the direct coupling of microwave energy with the molecular dipoles of the polar solvent, ethanol (boiling point about 78°C) undergoes instantaneous boiling and evaporation [19].

UV–vis optical characterization

UV–Vis absorption spectra of curcuminoids, graphite, and IGC solutions were recorded to analyze optical absorption behavior. The optical band gap was estimated using the Tauc plot method, while spectral deconvolution was performed to resolve overlapping absorption bands and identify individual electronic transitions. These analyses provide insight into the electronic structure modification and charge-transfer potential of the graphite–turmeric extract system. To estimate curcuminoid contents (E_i) from UV-Vis spectra, we can use the area under the curve (AUC) principle [25].

$$\%E_i = \frac{Peak\ Area}{Total\ Area} \times 100\% \quad (1)$$

The band gap is calculated by the Tauc plot as follows [26]–[28].

$$(\alpha h\nu)^{\gamma} = A\left(h\nu - E_g\right) \quad (2)$$

where ν is photon frequency, E_g is the band gap, A is the Tauc constant, h is Planck constant, c is light speed, α is the absorption coefficient, and γ is the transition factor ($\gamma = 2$ for a direct allowed transition or $\gamma = 0.5$ for an indirect allowed transition.

Electrochemical corrosion measurements

Electrochemical measurements were performed in a 3.5 wt% NaCl electrolyte using a two-electrode configuration with a Rodeostat open-source potentiostat (low-current configuration) [20]–[22]. The Zn electrode (coated with the inhibitor) served as the working electrode, while a high-purity graphite rod with a surface area ten times that of the working electrode was used as both the counter and pseudo-reference electrode. Prior to the measurements, the electrodes were immersed for 30 minutes to allow the system to reach a stable Open Circuit Potential (OCP). Linear Sweep Voltammetry (LSV) was performed using a potentiostat with a scan rate of 10 mV s^{-1} over a potential range from −1.0 V to +1.0 V [23], [24]. Note that this scan rate was initially selected to expedite the screening of various inhibitor compositions, which may introduce capacitive current contributions. Corrosion current density was obtained from Tafel extrapolation, and corrosion rates were calculated using standard electrochemical equations.

$$CR_i = \frac{KI_{corr}\ E_W}{n\rho} \quad (3)$$

where K is the conversion constant, I_{corr} is corrosion current, E_W is the equivalent weight, n is the number of electrons involved in the reaction, and ρ is the metal density. This approach is commonly used in corrosion studies of battery electrodes and stainless steel.

The corrosion inhibition efficiency (IE%) was then calculated by comparing the corrosion rates in the absence and presence of the inhibitor [4], as expressed in Equation (4),

$$IE\% = \left(\frac{CR_0 - CR_i}{CR_0}\right) \times 100\% \quad (4)$$

where CR_0 is the corrosion rate without inhibitor, and CR_i is the corrosion rate with inhibitor.

Result and Discussion

UV–Vis absorption spectra

The UV–Vis absorption spectra reveal distinct optical characteristics among the pristine curcuminoids, graphite, and the graphite–curcuminoids inhibitor (IGC) system, as depicted in Figure 2. To accommodate the wide variation in absorbance scales between the pristine and composite formulations, a dual y-axis plot is used in Figure 2, with the left axis for the composite systems and the right axis for the pristine components. Graphite exhibits strong absorption in the ultraviolet region with a tail extending into the visible range, which is characteristic of π–π* electronic transitions in sp^2-hybridized [9]. Such behavior is consistent with the broad optical absorption characteristics typically observed in graphitic carbon materials [29].

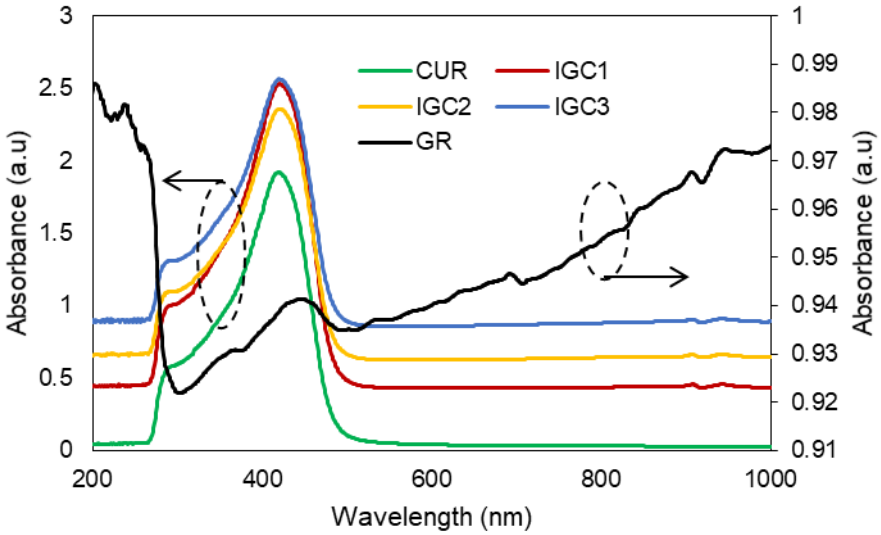

Figure 2. UV–Vis absorbance spectra of graphite (GR), curcuminoids (CUR), and graphite–curcuminoids inhibitor solutions (IGC1–IGC3). The left y-axis corresponds to the absorbance values of CUR and the hybrid systems (IGC1–IGC3), whereas the right y-axis corresponds to the absorbance values of GR.

Curcuminoids show a pronounced absorption band centered around 420 nm, which is attributed to π–π* and n–π* transitions within its conjugated aromatic structure and β-diketone functional groups [9]. After incorporating curcuminoids into the graphite-based

inhibitor solutions (IGC1–IGC3), noticeable changes in absorbance intensity and subtle spectral shifts are observed. These changes may indicate electronic interactions between curcuminoid molecules and the graphite surface, potentially involving π–π stacking interactions and weak hydrogen bonding [30].

The absorbance profiles of IGC1 and IGC3 display comparable peak intensities despite their different graphite contents (Table 1), as shown in Figure 2. This behavior suggests that increasing the graphite concentration does not necessarily result in a proportional increase in absorbance. One possible explanation is the limited dispersion capability of the carbon sheets within the fixed volume of the curcuminoid matrix [31]. At higher graphite loading, particle aggregation and light-scattering effects may reduce the contribution of additional graphite to the overall absorption response.

The changed absorbance intensity of the IGC systems compared to pristine curcuminoids indicates that the physical combination of components alters the transition state energy distributions, broadening the optical absorption properties [32]. Although UV–Vis spectroscopy alone cannot directly confirm the adsorption mechanism responsible for corrosion protection, these spectral changes provide evidence of interactions between the components that may facilitate their adsorption and film-forming behavior on metallic surfaces.

Optical band gap estimation

The optical band gap energy (E_g) of the prepared samples was estimated using the Tauc relation by plotting $(\alpha h\nu)^{\gamma}$ versus photon energy ($h\nu$) as shown in Figure 3. The linear region of the curve was extrapolated to the photon-energy axis to determine E_g by assuming a direct allowed transition. The optical band gap of graphite is approximately 2.85 eV (see Table 2). This value can be associated with electronic transitions in dispersed or partially oxidized graphite within the liquid solvent [9]. In contrast, pristine curcuminoids show a lower band gap (2.65 eV), consistent with their nature as an organic semiconductor with an extended π-conjugated system [31].

Table 2. Optical band gap values estimated using Tauc plots

Sample	Eg (eV)
CUR	2.65
GR	2.85
IGC1	2.62
IGC2	2.60
IGC3	2.59

A gradual decrease in band gap from 2.62 to 2.59 eV is observed for the graphite–curcuminoids inhibitor systems (IGC1–IGC3). Although the change is relatively small, it suggests that combining graphite with curcuminoids alters the system's optical response. This reduction in E_g suggests a modification of the electronic structure due to interactions between curcuminoid molecules and the graphite surface, which can influence the distribution of electronic states near the absorption edge [33]. Similar trends have been reported for various carbon–organic

hybrid materials, in which physical interactions between the constituents result in slight shifts in the optical band gap [34].

From a corrosion inhibition perspective, the reduced band gap may indicate a more favorable electronic environment for charge-transfer processes at the metal–solution interface[35]. In general, materials with lower band gap energies are often associated with enhanced electron-donating capability and stronger adsorption tendencies, which may contribute to the formation of protective layers on metallic surfaces [34]. However, the exact adsorption mechanism and the nature of the interactions with the zinc surface require further investigation using complementary electrochemical characterization.

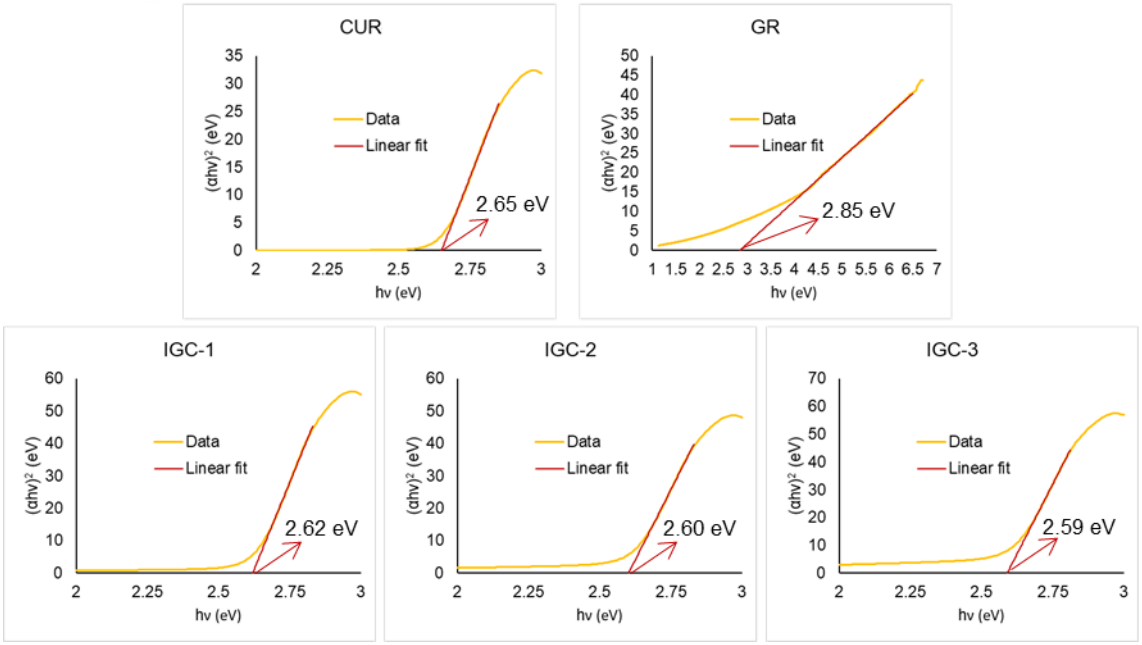

Figure 3. Tauc plot analysis used to estimate the optical bandgap energy (E_g). The linear fitting indicates that all samples exhibit direct allowed electronic transitions.

Deconvolution of UV–Vis absorption spectra

Spectral deconvolution of the UV–Vis absorption spectra was performed using Gaussian fitting functions to resolve overlapping bands and identify the major absorption components, as shown in Figure 4. Pristine curcuminoids exhibits five distinct absorption peaks, which are commonly associated with overlapping electronic transitions involving π→π* and n→π* excitations originating from aromatic rings, conjugated double bonds, and carbonyl groups [33], [36]. The presence of multiple absorption components indicates the complex electronic structure of the curcuminoid chromophores.

Compared with pristine curcuminoids, the graphite–curcuminoids systems shows noticeable changes in the deconvoluted spectral profiles, with the disappearance of intermediate-energy transitions [36]. This difference suggests that the presence of graphite influences the optical response of the system and may alter the relative contributions of individual electronic transitions. Similar spectral changes have been reported in carbon–organic hybrid materials [12], [36], where intermolecular interactions and local structural environments affect the

overall absorption characteristics. However, the exact nature of these interactions cannot be established solely from UV–Vis analysis.

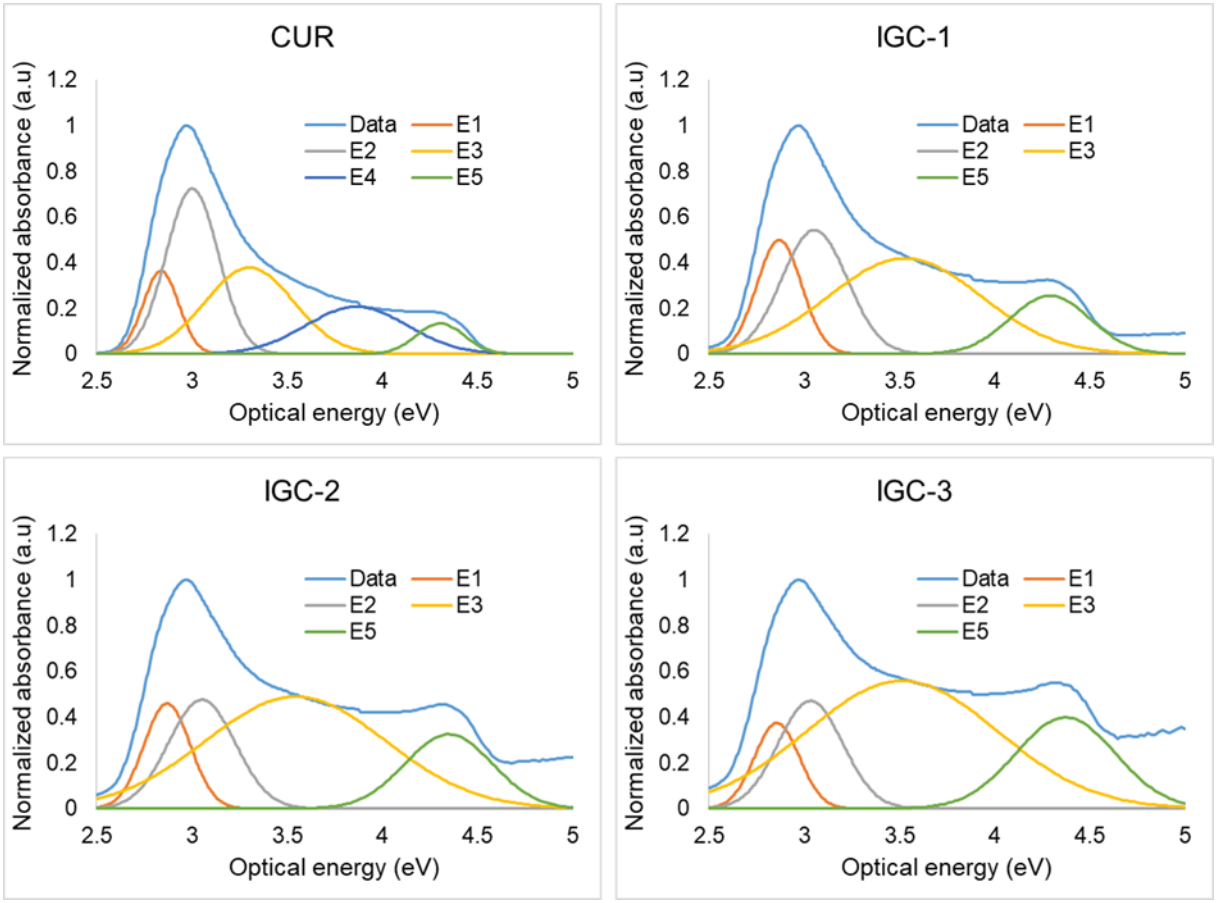

Figure 4. Deconvolution of UV–Vis absorption spectra of curcuminoids and graphite–curcuminoid inhibitor solutions.

Peak energy absorption from deconvolution analysis

The quantitative results obtained from the Gaussian deconvolution analysis are summarized in Tables 3 and 4. Table 3 show that the primary low-energy transitions (E1–E3) remain relatively stable after the formation of graphite–curcuminoids inhibitor systems, with only minor shifts toward higher energies. These modest shifts show the changes in the local electronic environment and interfacial interactions between curcuminoids and graphite. In particular, the lowest-energy component (E1 ~2.84–2.87 eV) remains almost constant across all samples, indicating that the principal chromophoric features of the curcuminoid extract are retained in the hybrid systems.

The relative contribution of each component was quantified using the area under the curve (AUC) approach described in Equation (1), in which the area of an individual peak was normalized to the total integrated area. For example, in pristine curcuminoids, the E1 and E3 components account for approximately 33.9% and 30.1% of the total spectral area, respectively. This finding also support that curcumin it associated compounds are the dominant chromophore in the turmeric extract (see Table 4). After the incorporation of graphite, changes

in the normalized peak areas are observed, indicating that the distribution of optical transitions within the hybrid system differs from that of the pristine organic phase [5].

Table 3. Peak energy absorption values obtained from deconvolution analysis

Sampel	E1 (eV)	E2 (eV)	E3 (eV)	E4 (eV)	E5 (eV)
CUR	2.84	3.00	3.30	3.87	4.30
IGC1	2.87	3.05	3.53	-	4.29
IGC2	2.87	3.05	3.54	-	4.35
IGC3	2.86	3.03	3.51	-	4.37

Table 4. UV-Vis spectral deconvolution parameters of the turmeric extract (CUR)

Parameter	E1	E2	E3	E4	E5
Center-band (eV)	2.84	3.00	3.30	3.87	4.30
Area	2.75	8.05	7.15	4.46	1.37
Height	11.76	23.44	12.24	6.71	4.36
FWHM	0.22	0.32	0.55	0.62	0.29
%Area	11.6	33.85	30.07	18.76	5.76

Interestingly, Table 3 shows that the intermediate-energy component E4 (3.87 eV), which is clearly resolved in the pristine CUR extract, is no longer distinguishable in the spectra of the hybrid systems (IGC1–IGC3). This observation suggests that incorporating graphite modifies the relative contributions and the overlap among the absorption components. One possible explanation is that interactions within the hybrid matrix broaden or merge certain transitions, making individual features less distinguishable after deconvolution [37]. In contrast, the high-energy component (E5 ~4.30–4.37 eV) remains observable in all samples, indicating that the higher-energy absorption features are largely preserved upon hybridization.

Tafel polarization curves

The potentiodynamic polarization curves shown in Figure 5 illustrate the influence of the different inhibitor formulations on the electrochemical behavior of the zinc electrode. The uninhibited sample exhibits the highest current density and well-defined anodic and cathodic branches, indicating active corrosion in the salt solution. The addition of the single-component inhibitors, namely curcuminoids (CUR) and graphite (GR), results in only slight changes in the polarization profiles. In contrast, the IGC1 formulation produces a noticeable decrease in current density and modifies both the anodic and cathodic branches. The relatively small shift in corrosion potential suggests that IGC1 behaves as a mixed-type inhibitor, affecting both anodic metal dissolution and cathodic reduction reactions [31].

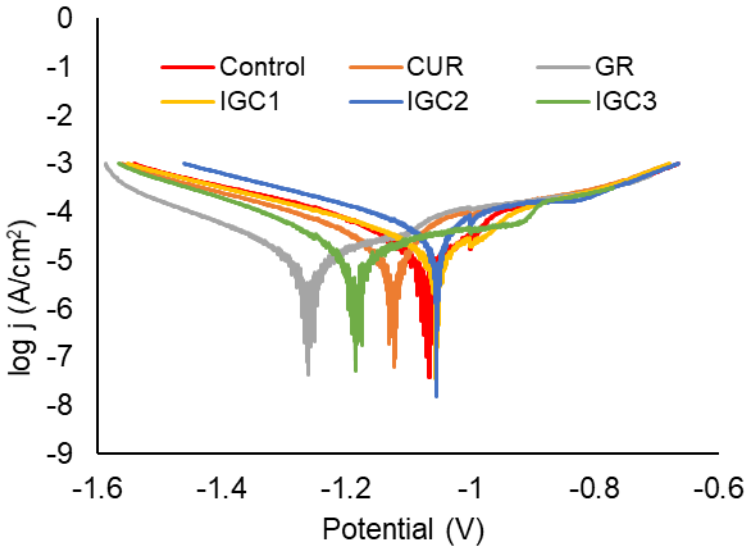

Figure 5. Tafel polarization curves of Zn in 3.5 wt% NaCl solution with different inhibitor systems.

Differences among the polarization curves become more apparent for the hybrid formulations. Compared with IGC1, the IGC2 sample exhibits a higher current density and a different polarization profile, whereas IGC3 shows an intermediate behavior. These variations indicate that the electrochemical response of the zinc electrode is sensitive to the composition of the graphite–curcuminoids system, with each formulation influencing the anodic and cathodic processes to different extents [23].

Corrosion rate of Zn

The potentiodynamic polarization parameters, including corrosion potential (E_{corr}), corrosion current density (i_{corr}), and anodic/cathodic Tafel slopes (β_a, β_c), are summarized in Table 4. The control sample without inhibitor exhibits a corrosion rate of 0.1175 mm/y, indicating the susceptibility of Zn to salt-induced corrosion [38], [39]. The experimental results reveal that the addition of inhibitors influences the electrochemical kinetics of Zinc disolution. The application of single-component inhibitors, curcuminoids (CUR) and graphite (GR), results in only modest reductions in corrosion rate, with inhibition efficiencies of 19.8% and approximately 11.6%, respectively. This indicates that each component alone provides limited protection under the present experimental conditions.

Table 4. Corrosion rate of Zn in 3.5 wt% NaCl solution in the presence of different inhibitors

Sample	V_{corr} (V)	i_{corr} (μA/cm²)	β_c	β_a	Corrosion rate, CR(mm/y)	IE(%)
Control	-1.0623	7.8476	-8.1727	10.3298	0.1175	-
CUR	-1.1184	6.2912	-10.1441	18.1929	0.0942	19.8
GR	-1.2606	6.9394	-7.4445	5.9935	0.1039	11.6
IGC1	-1.0555	2.7276	-22.3321	22.5965	0.0408	**65.3**
IGC2	-1.0514	12.4451	-11.5706	21.1093	0.1863	-58.6
IGC3	-1.1807	6.5627	-10.0486	8.0735	0.0983	16.3

Among the investigated formulations, the graphite–curcuminoids hybrid system with the IGC1 composition exhibits the best corrosion protection performance. The corrosion rate decreases to 0.0408 mm/y, corresponding to an inhibition efficiency of 65.3%. This improvement is accompanied by noticeable changes in both the anodic and cathodic Tafel slopes (β_a = 22.59 V/dec and β_c = 22.33 V/dec), suggesting that the inhibitor affects both anodic and cathodic reactions [40]. The improvement of IGC1 performance may be related to a favorable combination of graphite and curcuminoids, which facilitates the formation of a more effective protective layer on the zinc surface [41], [42].

In contrast, sample IGC2 shows a higher corrosion rate of 0.1863 mm/y, exceeding that of the control sample. This result indicates that the selected composition does not provide effective surface protection under the present conditions. One possible explanation is that higher graphite loading adversely affects the homogeneity of the deposited layer, thereby reducing its protective capability [43]. However, the exact origin of this behavior requires further investigation using additional surface and electrochemical characterization techniques, which we will save for future work.

When the graphite content was increased in IGC3, the inhibition efficiency became positive again (16.3%), with a corresponding corrosion rate of 0.0983 mm/year. This phenomenon indicates that the corrosion performance of the graphite-curcuminoid system is sensitive to changes in the composition of the hybrid inhibitor. Therefore, adjusting the compositional balance between turmeric extract and graphite seems to be crucial for achieving effective corrosion protection [15], [42].

Conclusion

This study demonstrates that the combination of curcuminoids and graphite forms an effective dual corrosion inhibitor system for zinc in a salty medium. UV–Vis absorption analysis reveals modifications in the optical properties of the graphite–curcuminoid hybrid systems, including changes in absorbance intensity, bandgap narrowing, and the distribution of optical transitions, as confirmed by spectral deconvolution. Electrochemical measurements using Tafel polarization analysis indicate that the corrosion-inhibition performance strongly depends on the inhibitor composition. The IGC1 formulation exhibited the highest inhibition efficiency (65.3%) and a mixed-type inhibition pattern. The comparison between the optical and electrochemical results suggests that both the electronic characteristics and the compositional balance of the dual systems influence their corrosion performance. In contrast, excessive graphite loading resulted in inferior protection, indicating that optical properties alone do not determine inhibition efficiency. This work provides valuable insights for the rational design of carbon–organic hybrid inhibitors for corrosion protection in salty solutions. However, future work should incorporate electrochemical impedance spectroscopy (EIS) and advanced surface analysis (SEM/XPS) to further elucidate the molecular adsorption mechanisms and long-term durability

Acknowledgment

The authors gratefully acknowledge the Institute for Research and Community Service (LPPM) of Universitas Muhammadiyah Riau (UMRI) for financial support of this research under the scheme “Penelitian Dosen Pemula” with Contract No. 39/PRJ/II.3.AUF/7/2025.

References

[1] W. H. Guan *et al.*, "Approaching the theoretical capacity limit of Na2FeSiO4-based cathodes with fully reversible two-electron redox reaction for sodium-ion battery," *Mater. Today Nano*, vol. 12, p. 100098, Dec. 2020.

[2] H. S. Hirsh, Y. Li, D. H. S. Tan, M. Zhang, E. Zhao, and Y. S. Meng, "Sodium-Ion Batteries Paving the Way for Grid Energy Storage," *Adv. Energy Mater.*, vol. 10, no. 32, Aug. 2020.

[3] C. Vaalma, D. Buchholz, M. Weil, and S. Passerini, "A cost and resource analysis of sodium-ion batteries," *Nat. Rev. Mater.*, vol. 3, no. 4, p. 18013, Mar. 2018.

[4] E. A. Flores-Frias, V. Barba, M. A. Lucio-Garcia, R. Lopez-Cecenes, J. Porcayo-Calderon, and J. G. Gonzalez-Rodriguez, "Use of Curcuma and Curcumin as Green Corrosion Inhibitors for Carbon Steel in Sulfuric Acid," *Int. J. Electrochem. Sci.*, vol. 14, no. 6, pp. 5026–5041, Jun. 2019.

[5] R. Wada, S. Takahashi, H. Muguruma, and N. Osakabe, "Electrochemical Detection of Curcumin in Food with a Carbon Nanotube- Carboxymethylcellulose Electrode," *Anal. Sci.*, vol. 36, no. 9, pp. 1113–1118, Sep. 2020.

[6] C. Verma, L. O. Olasunkanmi, E. E. Ebenso, and M. A. Quraishi, "Substituents effect on corrosion inhibition performance of organic compounds in aggressive ionic solutions: A review," *J. Mol. Liq.*, vol. 251, pp. 100–118, Feb. 2018.

[7] H. Ahmad, K. T. Kubra, A. Butt, U. Nisar, F. J. Iftikhar, and G. Ali, "Recent progress, challenges, and perspectives in the development of solid-state electrolytes for sodium batteries," *J. Power Sources*, vol. 581, p. 233518, Oct. 2023.

[8] M. N. Majeed and Q. A. Yousif, "Graphite-Enhanced TiO2 Nanoparticles Protect Duplex Stainless Steel against Acidic Corrosion," *J. Nanostructures*, vol. 12, no. 3, 2022.

[9] B. Alharbi, N. Aljeaban, A. Busaleh, and T. A. Saleh, "Efficient Corrosion Inhibition Using Graphene Oxide-Based Structures," *Mater. Perform.*, vol. 63, no. 7, pp. 40–43, Jul. 2024.

[10] G. Tatrari *et al.*, "Mass production of metal-doped graphene from the agricultural waste of Quercus ilex leaves for supercapacitors: inclusive DFT study," *RSC Adv.*, vol. 11, no. 18, pp. 10891–10901, 2021.

[11] C. W. Lee, S. Y. Jeong, Y. W. Kwon, J. U. Lee, S. C. Cho, and B. S. Shin, "Fabrication of laser-induced graphene-based multifunctional sensing platform for sweat ion and human motion monitoring," *Sensors Actuators A Phys.*, vol. 334, p. 113320, 2022.

[12] J. Lee and D. Berman, "Inhibitor or promoter: Insights on the corrosion evolution in a graphene-protected surface," Carbon, *N. Y.*, vol. 126, pp. 225–231, Jan. 2018.

[13] J. L. Gómez-Urbano, G. Moreno-Fernández, M. Arnaiz, J. Ajuria, T. Rojo, and D. Carriazo, "Graphene-coffee waste derived carbon composites as electrodes for optimized lithium ion capacitors," *Carbon N. Y.*, vol. 162, pp. 273–282, 2020.

[14] F. J. M *et al.*, "Optimizing anatase TiO_2 through aluminum doping: A comprehensive study for enhanced dye-sensitized solar cell performance," *Next Mater.*, vol. 9, p. 101006,

2025, doi: 10.1016/J.NXMATE.2025.101006.

[15] M. Pourmohseni, A. Rashidi, and M. Karimkhani, "Preparation of corrosion inhibitor from natural plant for mild steel immersed in an acidic environment: experimental and theoretical study," *Sci. Rep.*, vol. 14, no. 1, p. 7937, Apr. 2024.

[16] C. Liu *et al.*, "Rapid microwave activation of waste palm into hierarchical porous carbons for supercapacitors using biochars from different carbonization temperatures as catalysts," *RSC Adv.*, vol. 9, no. 34, pp. 19441–19449, 2019.

[17] K. R. Ahammed *et al.*, "Microwave-assisted synthesis of zinc oxide (ZnO) nanoparticles in a noble approach: utilization for antibacterial and photocatalytic activity," *SN Appl. Sci.*, vol. 2, no. 5, p. 955, May 2020.

[18] Z. Dong, T. Li, X. Xu, Y. Chen, J. Fu, and S. Sun, "Microwave-Assisted Preparation of Hierarchical Porous Carbon Aerogels Derived from Food Wastes for Supercapacitors," *Nanomaterials*, vol. 15, no. 5, p. 387, Mar. 2025.

[19] J. C. Assaf, Z. Mortada, S. A. Rezzoug, Z. Maache-Rezzoug, E. Debs, and N. Louka, "Comparative Review on the Production and Purification of Bioethanol from Biomass: A Focus on Corn," *Processes*, vol. 12, no. 5. 2024.

[20] H. J. Kwon *et al.*, "Development of smartphone-based ECL sensor for dopamine detection: Practical approaches," *Results Chem.*, vol. 2, 2020.

[21] T. Aryani, R. Roto, and M. Mudasir, "High-performance electrocatalytic degradation of crystal violet using graphene hydroxide-modified PbO2 electrode," *Results Chem.*, vol. 17, 2025.

[22] U. Matpal, H. Basheer, V. Bharadwaj, M. Samim, C. S. Azad, and I. A. Khan, "Cu–Kanamycin complex anchored on graphene oxide (Cu-kana@GO) for aqueous C–N and C–C coupling: A multifunctional recyclable nano catalyst," *Next Mater.*, vol. 10, 2026.

[23] C. Bao *et al.*, "Improved corrosion inhibition effect of a green three-component compound to Q235 steel in acidic solution," *Results Chem.*, vol. 15, p. 102316, May 2025.

[24] H. Zhao, S. Deng, Y. Qiang, J. Xu, D. Xu, and X. Li, "Synergistic mixture of Camellia Oleifera shell extract and KI as an eco-friendly and highly efficient composite inhibitor for steel corrosion in H2SO4 media," *J. Mol. Liq.*, vol. 407, p. 125164, Aug. 2024.

[25] J. Iacovacci, F. Palorini, A. Cicchetti, C. Fiorino, and T. Rancati, "Dependence of the AUC of NTCP models on the observational dose-range highlights cautions in comparison of discriminative performance," *Phys. Medica*, vol. 113, 2023.

[26] V. Mursyalaat, V. I. Variani, W. O. S. Arsyad, and M. Z. Firihu, "The development of a program for calculating the band gap energy of semiconductor material based on UV-Vis spectrum using Delphi 7.0," *J. Phys. Conf. Ser.*, vol. 2498, no. 1, p. 012042, May 2023.

[27] A. Z. Johannes, R. K. Pingak, and M. Bukit, "Tauc Plot Software: Calculating energy gap values of organic materials based on Ultraviolet-Visible absorbance spectrum," *IOP Conf. Ser. Mater. Sci. Eng.*, vol. 823, no. 1, p. 012030, Apr. 2020.

[28] P. R. Jubu *et al.*, "Comment about the use of unconventional Tauc plots for bandgap energy determination of semiconductors using UV–Vis spectroscopy," *Results Opt.*, vol. 14, 2024.

[29] N. Sofyan, A. M. Jamil, A. Ridhova, A. H. Yuwono, D. Dhaneswara, and J. W. Fergus, "Graphene oxide doping in tropical almond (Terminalia catappa L.) fruit extract mediated green synthesis of TiO2 nanoparticles for improved DSSC power conversion efficiency," *Heliyon*, vol. 10, no. 8, p. e29370, 2024.

[30] Z. Liu, A. Quek, and R. Balasubramanian, "Preparation and characterization of fuel pellets from woody biomass, agro-residues and their corresponding hydrochars," *Appl. Energy*, vol. 113, 2014.

[31] A. F. Betancur-Lopera *et al.*, "Role of low-dimensional carbon nanostructures in hybrid material as anticorrosive coating," *Prog. Org. Coatings*, vol. 163, p. 106682, Feb. 2022.

[32] K. P. Raj *et al.*, "Influence of Mg Doping on ZnO Nanoparticles for Enhanced Photocatalytic Evaluation and Antibacterial Analysis," *Nanoscale Res. Lett.*, vol. 13, p. 229, 2018.

[33] L. Chen, D. Lu, and Y. Zhang, "Organic Compounds as Corrosion Inhibitors for Carbon Steel in HCl Solution: A Comprehensive Review," *Materials (Basel)*, vol. 15, no. 6, p. 2023, Mar. 2022.

[34] H. He *et al.*, "Exploring green and efficient zero-dimensional carbon-based inhibitors for carbon steel: From performance to mechanism," *Constr. Build. Mater.*, vol. 411, p. 134334, Jan. 2024.

[35] R. Salim *et al.*, "Corrosion inhibition and adsorption mechanism of novel imidazopyridine corrosion inhibitors: Electrochemical and computational studies," *J. Ind. Eng. Chem.*, vol. 151, pp. 618–638, Nov. 2025.

[36] H. O. Dogan, F. Yıldırım, Z. Orhan, A. Ben Ahmed, M. Benhaliliba, and Ş. Aydoğan, "Numerical evaluations of curcumin organic molecule and an experimental study on hybrid photodetector performance in visible and UV regions," *Org. Electron*, vol. 124, p. 106946, Jan. 2024.

[37] L. T. Figueroa-Ariza and B. A. Paez-Sierra, "Solvent-dependent spectral deconvolution of amino-substituted chalcones: UV–vis and FT-IR analysis supported by TD-DFT calculations," *J. Mol. Struct.*, vol. 1351, 2026.

[38] A. Royani, M. Hanafi, A. Thakur, A. Zarrouk, N. M. Mubarak, and A. Manaf, "Electrochemical and computational investigation of Tinospora cordifolia fractions as a novel corrosion inhibitor for carbon steel in seawater medium," *Sci. Rep.*, vol. 15, no. 1, 2025.

[39] A. Royani, "Moringa oleifera Extract as a Green Corrosion Inhibitor for API 5L in Seawater Medium: Electrochemistry and Surface Study," *J. Bio- Tribo-Corrosion*, vol. 12, no. 2, p. 83, Jun. 2026.

[40] A. Marzaq *et al.*, "Environmentally-friendly imidazolium-derived ionic liquid as a corrosion inhibitor for carbon steel in 1 M HCl: experimental and theoretical approach," *J. Dispers. Sci. Technol.*, pp. 1–18, Jun. 2025.

[41] A. M. Guruprasad, H. P. Sachin, G. A. Swetha, and B. M. Prasanna, "Corrosion inhibition of zinc in 0.1 M hydrochloric acid medium with clotrimazole: Experimental, theoretical and quantum studies," *Surfaces and Interfaces*, vol. 19, p. 100478, Jun. 2020.

[42] T. R. Ovari, A. M. V. Brânzanic, G. Katona, G. S. Szabó, and L. M. Muresan, "New eco-friendly corrosion inhibitor for zinc based on expired Detralex drug. Adsorption, electrochemical and computational studies," *Mater. Today Commun.*, vol. 46, p. 112739, Jun. 2025.

[43] K. Shwetha, B. M. Praveen, and B. K. Devendra, "A review on corrosion inhibitors: Types, mechanisms, electrochemical analysis, corrosion rate and efficiency of corrosion inhibitors on mild steel in an acidic environment," *Results in Surfaces and Interfaces*, vol. 16, p. 100258, Aug. 2024.